Chinese Physics B



PAPER

# Graphene/$SrTiO_3$ interface-based UV photodetectors with high responsivity*

To cite this article: Heng Yue *et al* 2021 *Chinese Phys. B* **30** 038502

# Graphene/$SrTiO_3$ interface-based UV photodetectors with high responsivity*

Heng Yue(岳恒)[1,†], Anqi Hu(胡安琪)[1,†], Qiaoli Liu(刘巧莉)[1], Huijun Tian(田慧军)[1], Chengri Hu(胡成日)[1], Xiansong Ren(任显松)[1], Nianyu Chen(陈年域)[1], Chen Ge(葛琛)[2], Kuijuan Jin(金奎娟)[2,§], and Xia Guo(郭霞)[1,‡]

[1] *State Key Laboratory for Information Photonics and Optical Communications, School of Electronic Engineering, Beijing University of Posts and Telecommunications, Beijing* 100876, *China*

[2] *Beijing National Laboratory for Condensed Matter Physics, Institute of Physics, Chinese Academy of Sciences, Beijing* 100190, *China*

(Received 15 November 2020; revised manuscript received 25 December 2020; accepted manuscript online 11 January 2021)

Strontium titanate ($SrTiO_3$), which is a crucial perovskite oxide with a direct energy band gap of 3.2 eV, holds great promise for ultraviolet (UV) photodetection. However, the response performance of the conventional $SrTiO_3$-based photodetectors is limited by the large relative dielectric constant of the material, which reduces the internal electric field for electron-hole pair separation to form a current collected by electrodes. Recently, graphene/semiconductor hybrid photodetectors by van-der-Waals heteroepitaxy method demonstrate ultrahigh sensitivity, which is benefit from the interface junction architecture and then prolonged lifetime of photoexcited carriers. Here, a graphene/$SrTiO_3$ interface-based photodetector is demonstrated with an ultrahigh responsivity of $1.2\times10^6$ A/W at the wavelength of 325 nm and $\sim 2.4\times10^4$ A/W at 261 nm. The corresponding response time is in the order of $\sim$ ms. Compared with graphene/GaN interface junction-based hybrid photodetectors, $\sim$ 2 orders of magnitude improvement of the ultrahigh responsivity originates from a gain mechanism which correlates with the large work function difference induced long photo-carrier lifetime as well as the low background carrier density. The performance of high responsivity and fast response speed facilitates $SrTiO_3$ material for further efforts seeking practical applications.

**Keywords:** interface, $SrTiO_3$, ultraviolet photodetector, high responsivity

**PACS:** 85.30.Hi, 85.60.Bt, 85.60.Gz **DOI:** 10.1088/1674-1056/abda2e

## 1. Introduction

Two-dimensional (2D) material on top of semiconductor grown by van-der-Waals heteroepitaxy method, which enables interface junction to drive electrons and holes transport, currently serves as a major workhorse for photodetectors with ultrahigh responsivity. Graphene has turned out to be a widely utilized heteroepitaxy material among the 2D materials due to its ultrahigh transparency and ultrahigh mobility owing to its zero-mass nature in the linear $E$–$k$ dispersion relationship at low energy.[1,2] To establish the 2D/semiconductor photodetection architecture for efficient photocurrent amplification, there are mainly two routes that have been employed, including graphene on bulk semiconductor,[3–7] and graphene on nanostructures such as quantum dots and nanowires.[8–11] Limited by the small work function difference between graphene and semiconductor, or strong radiation recombination, which results in weak carrier local confinement at the interface, the photodetection performance based on graphene on bulk semiconductor structure is much lower than that of graphene on quantum dot structure. It was reported that the responsivity to 325 nm light was only about 5.83 A/W at $-10$ V for graphene/GaN,[12] $1.3\times10^3$ A/W at $-1$ V for graphene/GaAs photodetector to 650 nm incident light,[13] respectively. While replacement by graphene on quantum dot structure improves the responsivity by several orders of magnitude for the graphene/quantum dot photodetectors due to highly local confinement.[14–17] However, affected by the persistent photoconductivity effect caused by crystalline defects existed in the quantum dots, the transient response time can even be as long as several hours. Hence, it is desirable to search for a structure with a highly crystalline structure as well as strong carrier confinement for high photodetection performance.

Ultraviolet (UV) light detection has drawn a great deal of attention in civil and military applications such as solar astronomy, short-range communications security, biological research, fire alarms, and military services.[18–22] Especially, detection of deep-UV light with wavelengths lower than 280 nm has stronger anti-interference ability due to the low environmental background in this spectral range. Wide band gap semiconductors opened the possibility for high performance UV detectors due to their intrinsic visible/solar blind prop-

*Project supported by the National Key Research and Development Program of China (Grant Nos. 2017YFF0104801 and 2018YFB0406601) and the National Natural Science Foundation of China (Grant Nos. 61804012 and 11721404).

†These authors contributed equally.

‡Corresponding author. E-mail: guox@bupt.edu.cn

§Corresponding author. E-mail: kjjin@iphy.ac.cn

 

erty. Strontium titanate ($SrTiO_3$) is a crucial perovskite oxide with an energy band gap of $\sim 3.2$ eV,[23] which holds great promise for ultraviolet (UV) photodetection. However, the quantum efficiency of $SrTiO_3$ photodetector is relatively low, which results from the large relative dielectric constant of the material ($\sim$310 even at room temperature) due to the low-energy phonon mode.[24] For conventional PIN and Schottky photodiodes, the maximum electric field is correlated with $1/(\varepsilon_r\varepsilon_0)^{1/2}$, where $\varepsilon_r$ is the relative dielectric constant, $\varepsilon_0$ is the dielectric constant of vacuum. As $\varepsilon_r$ for $SrTiO_3$ is several hundred times larger than other wide band gap materials such as GaN and SiC, the electric field inside $SrTiO_3$ is very low. Because effective photodetection is based on the separation and transport of photogenerated electron-hole pairs under an electric field, the low electric field inside $SrTiO_3$ lowers its photon response performance. Many methods were proposed for enhancing the electric field intensity between electrodes, such as applied high voltage between source-drain electrodes.[25] The responsivity of most $SrTiO_3$-based devices is limited to hundreds of mA/W, and the maximum reported responsivity is 46.1 A/W as far as we know.[26]

In this work, a graphene/$SrTiO_3$ interface based photodetector is demonstrated, in which $SrTiO_3$ is the light absorbing material and graphene is the carrier transport material taking advantage of its high carrier mobility. Owing to the gain mechanism enhanced by the large work function between graphene and $SrTiO_3$ in this structure, the high responsivity of $1.2\times10^6$ A/W at 325 nm incident light and $2.4\times10^4$ A/W at 261 nm incident light is achieved despite the large dielectric constant property of $SrTiO_3$, which is more than two orders larger than graphene/GaN at 325 nm and five times larger than graphene/GaN at 261 nm, respectively.

## 2. Experimental details

**Device fabrication** Figure 1(a) presents the schematic structure of hybrid graphene/$SrTiO_3$ photodetector. The $SrTiO_3$ substrate in the present study was an as-supplied single polished $SrTiO_3$ (100) single crystal with a purity of 99.99% and a thickness of 0.5 mm. After cleaned in acetone and ethanol solution twice, standard lithography and etching processes were performed to define the contact pattern. Then a Ni/Au (15 nm/300 nm) electrode was deposited by magnetron sputtering to form a good ohmic contact with $SrTiO_3$ and treated by rapid thermal annealing at 450 ℃ for 30 s in $N_2$. The electrode size was 100 μm × 200 μm with the photosensitive area of about 0.02 $mm^2$.

Polymethylmethacrylate (PMMA) was spun on the monolayer graphene, which was grown on 25-μm-thick Cu foil by chemical vapor deposition (CVD) method, and heated for 25 min at 150 ℃ to ensure the combination tighter. Then it was soaked in $FeCl_3$ for three hours to etch the Cu foil to guarantee the graphene transferred to PMMA. Subsequently, the graphene on PMMA was transferred to deionized water to dilute $FeCl_3$ and then transferred to the target substrate. After that, it was soaked in acetone for four hours to resolve the PMMA and washed in acetone, ethanol, deionized water gently again. At last, heated it 20 min at 60 ℃ to evaporate the water, the device fabrication is completed.

**Measurement method** Raman spectroscopy was conducted to characterize the quality of graphene after van-der-Waals epitaxy with an excitation wavelength of 514 nm (Renishaw). The Hall measurement was carried out using the Van der Pauw Hall test method to evaluate the doping type, carrier concentration, and carrier mobility of the transferred graphene.

**Device characterization** Photoelectric measurements were performed using a semiconductor parameter analyzer (Keithley 4200) under light illumination at various powers in a dark room at room temperature. A series of attenuators were applied to attenuate the 325 nm and 261 nm laser light intensity. These devices were wire-bonded on a printed circuit board for the measurements. The time response was recorded by the oscilloscope ROHDE&SCHWARZ RTM2054.

## 3. Results and discussion

Raman measurement result of graphene-on-$SiO_2$ is shown in Fig. 1(b). Three dominant feature peaks of graphene are distinguished, which are the G band ($\sim$1586 $cm^{-1}$), the G* band ($\sim$2328 $cm^{-1}$), and the 2D band (2688 $cm^{-1}$). The G band is a zone-center mode with a phonon wave vector of $q=0$. The G* (iTO + LA $q\approx 2k$ and 2iTO $q\approx 0$) mode and the 2D (2iTO $q\approx 2k$) mode come from a double resonance Raman (DRR) process, where $k$ is the electron wave vector, and $q$ and $k$ are measured from the $K$ point of the Brillouin zone (BZ). Note the intensity ratio of the 2D peak to the G peak is above 4 and there is an absence of the D peak, indicating the experimental graphene is monolayer with high quality.[27] Besides, there is a blueshift of the tested 2D peak compared to pristine graphene (whose 2D peak is 2641 $cm^{-1}$), which indicates the graphene is initially P-type doped. Hall measurement of graphene on $SrTiO_3$ demonstrates a hole concentration of $1.26\times10^{13}$ $cm^{-2}$ at 300 K, which determines the Fermi-level 0.41 eV below the Dirac point according to the equation

$$n_g = (E_F/\hbar v_F)^2/\pi, \tag{1}$$

where $E_F$ is the Fermi energy, $\hbar$ is the Planck constant, and $v_F = 10^6$ m/s is the carrier group velocity in graphene. Owing to the work function difference (1.1 eV) between $SrTiO_3$ (5.7 eV)[23] and graphene (4.6 eV),[35] the band diagram is illustrated in Fig. 1(d).

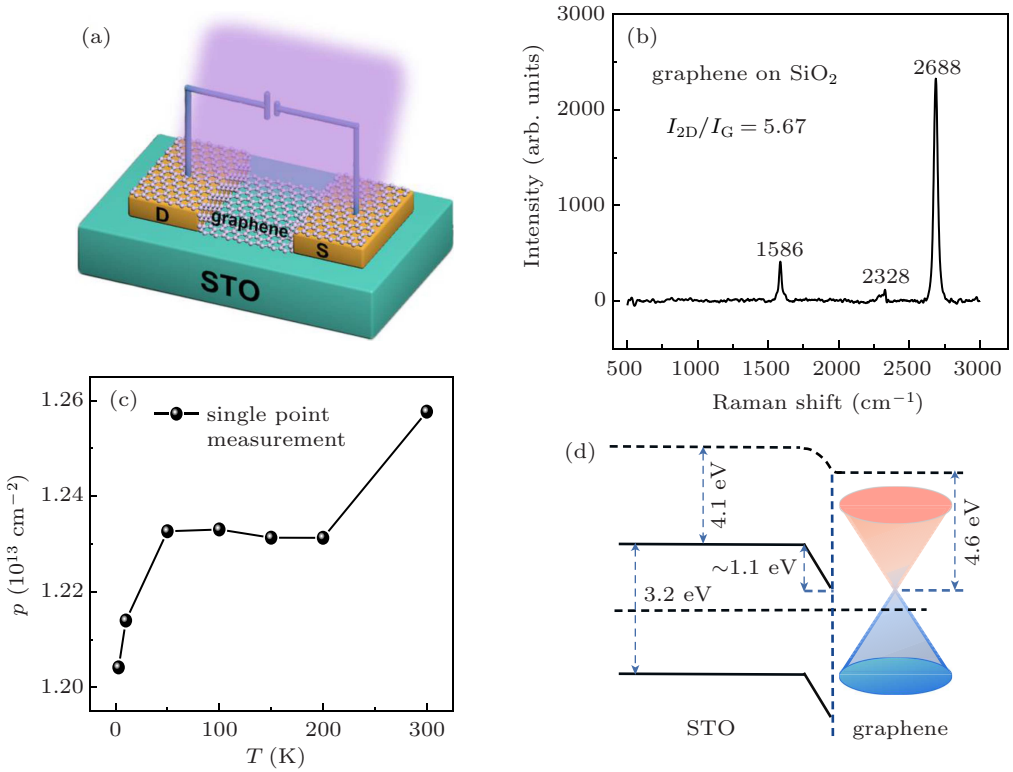


**Fig. 1.** (a) Schematic of the device structure. (b) Raman spectra of graphene on $SiO_2$. The absence of the D peak indicates the graphene keeps high quality with few defects after the transfer process. (c) Temperature-dependent Hall measurement of the device. (d) Schematic diagram of the band structures of graphene and $SrTiO_3$ after contact in the dark.

The photoelectric response performance of the graphene/$SrTiO_3$ photodetector is presented in Fig. 2. The photocurrent $I_{photo}$ (calculated by $I_{light} - I_{dark}$) increases linearly with the source-drain voltage under 325 nm light at different incident power (Fig. 2(a)). The photocurrent is a negative signal at positive bias, which means the conductance of graphene decreases with increasing incident power. The responsivity denoted by

$$R = I_{photo}/P_{in}, \tag{2}$$

where $P_{in}$ is the incident light power, is depicted as a function of the applied $V_{SD}$ in Fig. 2(b) (The absolute value of the responsivity is expressed in logarithm form.). The highest responsivity of $1.2 \times 10^6$ A/W is obtained at 1 V under the lowest incident power of 21.3 pW, which is more than four orders of magnitude higher than previously reported $SrTiO_3$ based photodetectors[28] and almost ten orders of magnitude higher than the device without graphene fabricated at the same time. More strikingly, this responsivity is two orders larger than graphene/GaN at 1 V we made at the same time for comparison (The graphene/GaN photodetector maximum responsivity obtained is $3.9 \times 10^3$ A/W with the minimum incident power of 180 pW at 325 nm and $4.7 \times 10^3$ A/W with the minimum incident power of 150 pW at 261 nm for graphene/UID-GaN hybrid photodetector). The corresponding photoconductive gain at 1 V is calculated to be $\sim 5 \times 10^6$ according to the equation

$$\text{Gain} = \frac{I_{photo}/e}{P_{in}/h\nu}, \tag{3}$$

where $e$ is the electron charge, $h$ is Planck's constant, $\nu$ is the incident photon frequency. The responsivity and gain (in logarithmic form) decrease with the incident power with the slop of $-0.72$. This qualitative mechanism can readily explain the inversion relation of the responsivity and the incident power.

Correspondingly, the specific detectivity ($D^*$) is calculated to be $3.5 \times 10^{10}$ Jones at room temperature, which determines the minimum illumination light power that a detector can distinguish from the noise, according to

$$D^* = \frac{\sqrt{A \cdot \Delta f}}{\text{NEP}}, \tag{4}$$

where $A$ is the effective area of the detector, $\Delta f$ is the electrical bandwidth in hertz, NEP is the noise equivalent power. The NEP is defined by

$$\text{NEP} = \langle I_n^2 \rangle^{1/2}/R, \tag{5}$$

where $R$ is the responsivity, and $\langle I_n^2 \rangle$ is the noise spectral density consisting of the $1/f$ noise, short noise, and thermal noise of the detector.[29,30] For such graphene/$SrTiO_3$ structure, $1/f$ noise, originated from the carrier trapping and detrapping processes at the graphene/$SrTiO_3$ interface, still dominates at low frequency and is considerably larger than shot noise and thermal noise.

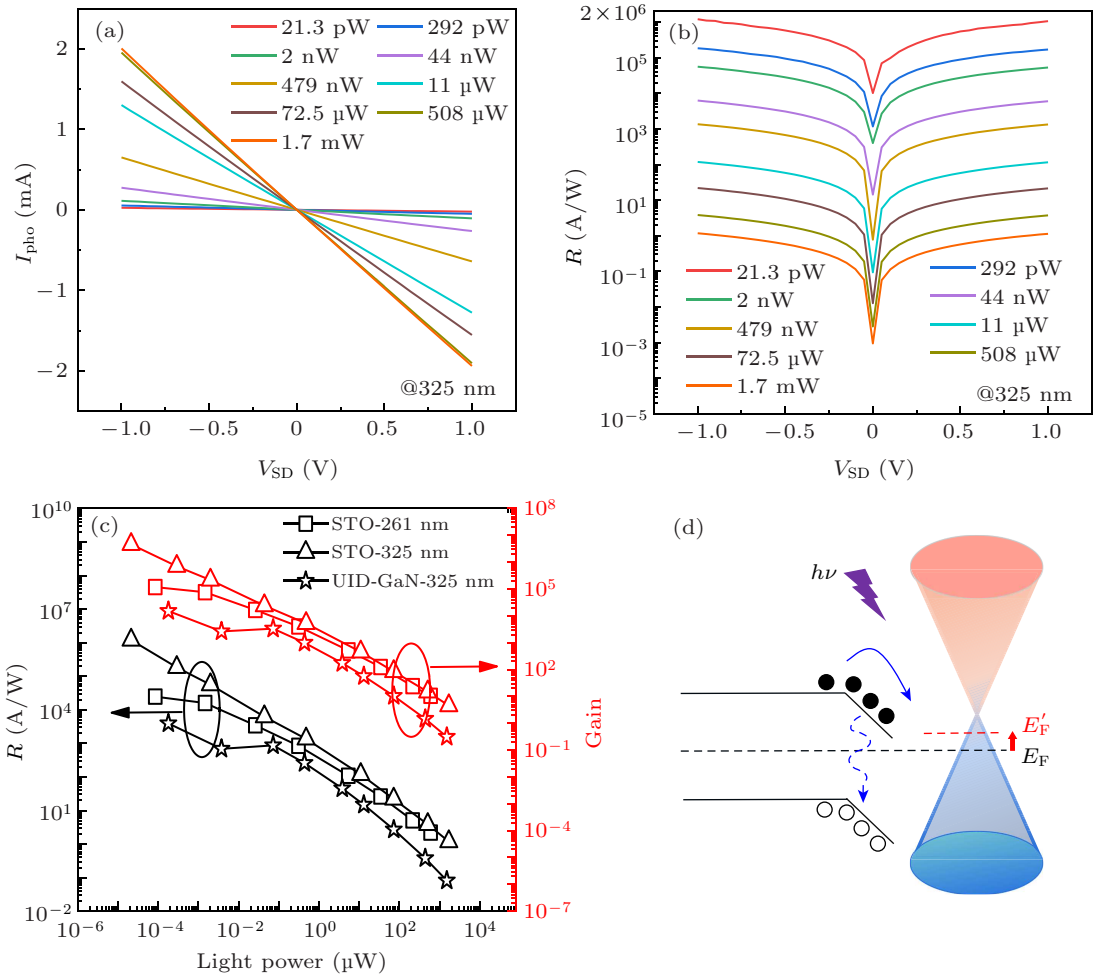


**Fig. 2.** (a) Photocurrent and (b) responsivity as a function of the bias under different incident power at 325 nm wavelength. (c) Comparison between graphene/$SrTiO_3$ and graphene/UID-GaN in responsivity and gain as a function of incident power at the bias of 1 V and the wavelengths of 325 nm and 261 nm. (d) Energy band diagram after illumination. The photo-generated electrons transferred to graphene and holes trapped in $SrTiO_3$ (the dotted arrow indicated the recombination occurred in $SrTiO_3$).

The photo response at 261 nm is also conducted. Because the energy of carriers excited by 261 nm is much larger than the band gap of $SrTiO_3$, part of the photo-excited carriers are capable of overcoming the barrier to the graphene layer, which diminishes the internal gain. The responsivity and gain is smaller than the response to 325 nm but can still reach high values of $2.4 \times 10^4$ A/W and $\sim 10^5$ under the lowest incident power of 85.1 pW. This result implies the graphene/$SrTiO_3$ photodetector can perform well at UV and deep-UV wavelengths.

The internal reason for the gain is the recirculation of the signal carriers in graphene during the lifetime of the remained photo-excited carriers in $SrTiO_3$. The physical expression of the gain is as follows:[31–34]

$$\text{Gain} = \tau_{\text{lifetime}}/\tau_{\text{transit}}, \tag{6}$$

where $\tau_{\text{lifetime}}$ is the remained photo-excited holes in $SrTiO_3$, $\tau_{\text{transit}}$ is the signal carrier transit time between the two electrodes in graphene. Attributed to the large work function difference between graphene and $SrTiO_3$, the barrier height for holes to escape from $SrTiO_3$ is large (as shown in Fig. 2(d)), making the holes trapped in $SrTiO_3$ and prolonging the $\tau_{\text{lifetime}}$. At the same time, the small $\tau_{\text{transit}}$ mainly depends on the high mobility of graphene when the electrode distance and bias voltage are defined. The long $\tau_{\text{lifetime}}$ and the short $\tau_{\text{transit}}$ jointly decide the high gain and the corresponding high responsivity. For comparison, measurements of photodetectors without graphene is also conducted, and the highest responsivity is just dozens of μA/W at 1 V applied bias. A significant improvement of responsivity of about $10^{10}$ times is obtained by the gain mechanism in devices with graphene.

Wurtzite GaN material with an energy bandgap of 3.4 eV is a promising material for UV photodetection. However, when comparing the photoresponse performance for graphene/UID-GaN and graphene/$SrTiO_3$ hybrid structure, as shown in Fig. 2(c), the responsivity result of $SrTiO_3$ is also much higher than that of GaN, which is kept at the same measurement condition. The maximum responsivity obtained is $3.9 \times 10^3$ A/W with the minimum incident power of 180 pW at

325 nm and $4.7 \times 10^3$ A/W with the minimum incident power of 150 pW at 261 nm for graphene/UID-GaN hybrid photodetector. The relatively low photoresponsivity is attributed to the small work function difference for graphene/UID-GaN structure, which is $\sim 0.5$ eV. Small work function difference at the interface results in inefficient separation of electron-hole pairs, which indicates a large recombination rate at the interface and then reduced lifetime. For graphene/p-GaN structure, the work function difference can be as high as 2.5 eV. However, the high density of holes as background also shortens the lifetime of photoexcited electrons through radiation recombination, which results in lower responsivity.[35]

As another key parameter to evaluate a photodetector performance, the response time of the photodetectors under different illumination powers was measured, and the curves were plotted in Fig. 3, which shows the transient photoresponse of the device when switching on/off the UV light of 325 nm wavelength and 261 nm wavelength. The response time consists of the rise time ($\tau_r$) and the decay time ($\tau_d$). The rise time is measured from 10 % to 90 % of the signal peak value, while the decay time is measured oppositely from 90 % to 10 %. It is seen from Figs. 3(a) and 3(b) that the response time decreases with the increasing illumination power. The $\tau_r$ and $\tau_d$ decreases from 19 ms and 22 ms under 5.3 μW illumination power to 6 ms and 15.3 ms under 508 μW illumination power at 325 nm. The faster response speed at higher illumination power is because it takes less time to balance the carrier generation and recombination rate. The response time evolution with the incident power at 261 nm illumination follows the same pattern as that at 325 nm. However, the rise time is larger. For example, $\tau_r$ of 36.9 ms under 805 μW at 261 nm is almost six times larger than that under 508 μW power at 325 nm. This is consistent with the fact that the photo carrier separation efficiency is lower because of the photon energy of 261 nm being much larger than the $SrTiO_3$ band gap, which promotes the carrier recombination, and it takes more time to reach the balanced state.

The responsivity and response speed are always two conflicting performances for such hybrid photodetectors. The figure of merit provides a comprehensive consideration of the two factors to evaluate the device performance, as shown in Fig. 3(c).[3,6,7,12,13,35–38] For a detailed comparison, the figures of merit are summarized for previously reported hybrid graphene/bulk semiconductor photodetectors. It can be seen the most significant advantage of this work is the higher responsivity due to the long $\tau_{lifetime}$ caused by the large work function difference of $SrTiO_3$ and graphene. Beyond that, the comprehensive performance is also quite favorable.

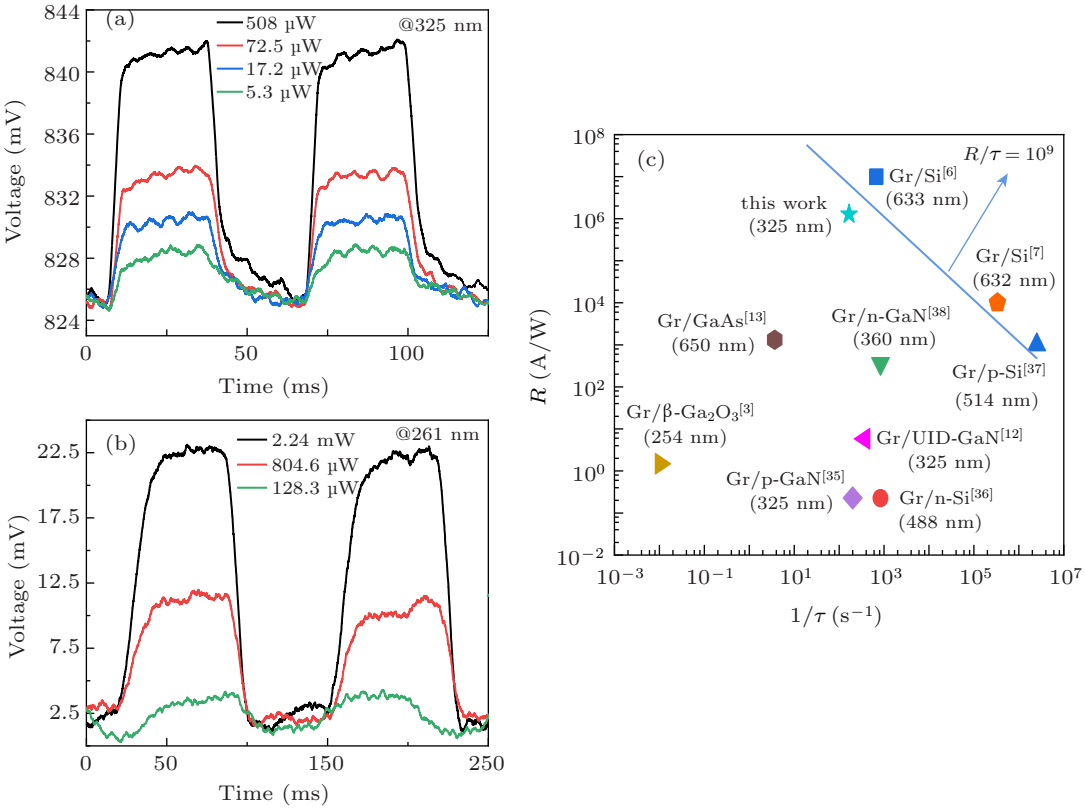


**Fig. 3.** Temporal response of the device under different illumination power at 325 nm wavelength (a) and 261 nm wavelength (b). (c) Comparison between response time and responsivity of our device and those of typical reported hybrid graphene/bulk semiconductor photodetectors, with the photoactive material adopted in the device, the corresponding reference number (in square brackets) and the operation wavelength (in parentheses) in each labeled text. Integration of graphene with low-dimensional materials, such as QD, nanowire, is not included.

## 4. Conclusion

In summary, a graphene/$SrTiO_3$ based photodetector demonstrating high responsivity performance at UV (325 nm) and deep-UV (261 nm) wavelengths is reported. The device design overcomes the shortcoming (the very large dielectric constant) of $SrTiO_3$ material for its application in the photodetector. The large work function between graphene and $SrTiO_3$ enhances the internal gain and the highest responsivity of $1.2\times10^6$ A/W under 21.3 pW illumination power at 325 nm and $2.4\times10^4$ A/W under 85.1 pW at 261 nm is achieved. The responsivity is almost $10^{10}$ times higher than the device without graphene. Nevertheless, they are two orders larger than graphene/GaN at 325 nm and more than five times larger than graphene/GaN at 261 nm, respectively. The response speed of the device is also characterized and the $\sim$ ms response speed is achieved. In addition, the excellent performance does not need a complicated manufacturing process or doping type of the substrate. This work paves a feasible way to develop new $SrTiO_3$ based UV photodetectors with high performance.

## References


[1] Xia F N, Mueller T, Lin Y M, Valdes-Garcia A and Avouris P 2009 *Nat. Nanotechnol.* **4** 839
[2] Lin F, Chen S W, Meng J, Tse G, Fu X W, Xu F J, Shen B, Liao Z M and Yu D P 2014 *Appl. Phys. Lett.* **105** 073103
[3] Kong W Y, Wu G A, Wang K Y, Zhang T F, Zou Y F, Wang D D and Luo L B 2016 *Adv. Mater.* **28** 10725
[4] Huang M Q, Wang M L, Chen C, Ma Z W, Li X F, Han J B and Wu Y Q 2016 *Adv. Mater.* **28** 3481
[5] Chen Z F, Li X M, Wang J Q, Tao L, Long M Z, Liang S J, Ang L K, Shu C, Tsang H K and Xu J B 2017 *ACS Nano* **11** 430
[6] Liu F Z and Kar S 2014 *ACS Nano* **8** 10270
[7] Chen Z F, Cheng Z Z, Wang J Q, Wan X, Shu C, Tsang H K, Ho H P and Xu J B 2015 *Adv. Opt. Mater.* **3** 1207
[8] Lu Y H, Wu Z Q, Xu W L and Lin S S 2016 *Nanotechnology* **27** 48LT03
[9] Zhang H, Babichev A V, Jacopin G, Lavenus P, Julien F H, Egorov A Y, Zhang J, Pauporté T and Tchernycheva M 2013 *J. Appl. Phys.* **114** 234505
[10] Boruah B D, Ferry D B, Mukherjee A and Misra A 2015 *Nanotechnology* **26** 235703
[11] Nie B, Hu J G, Luo L B, Xie C, Zeng L H, Lv P, Li F Z, Jie J S, Feng M, Wu C Y, Yu Y Q and Yu S H 2013 *Small* **9** 2872
[12] Tian H J, Liu Q L, Zhou C X, Zhan X J, He X Y, Hu A Q and Guo X 2018 *Appl. Phys. Lett.* **113** 121109
[13] Tian H J, Hu A Q, Liu Q L, He X Y and Guo X 2020 *Adv. Opt. Mater.* **8** 1901741
[14] Liu Q L, Tian H J, Li J, Hu A Q, He X Y, Sui M L and Guo X 2019 *Adv. Opt. Mater.* **7** 1900455
[15] Konstantatos G, Badioli M, Gaudrea L, Osmond J, Bernechea M, Arquer F P G, Gatti F and Koppens F H L 2011 *Nat. Nanotechnol.* **7** 363
[16] Adinolfi V and Sargent E H 2017 *Nature* **542** 324
[17] Kufer D, Nikitskiy I, Lasanta T and Navickaite G 2015 *Adv. Mater.* **27** 176
[18] Wang L, Jin K J, Xing J, Ge C, Lu H B, Zhou W J and Yang G Z 2013 *Appl. Opt.* **52** 3473
[19] Ohta H and Hosono H 2004 *Mater. Today* **7** 42
[20] Jiang H and Egawa T 2007 *Appl. Phys. Lett.* **90** 7115
[21] Tuta T, Yelboga T, Ulker E and Ozbay E 2008 *Appl. Phys. Lett.* **92** 7433
[22] Zhang Y, Shena S, Kim H J, Choi S, Ryou J, Dupuis R D and Narayan B 2009 *Appl. Phys. Lett.* **94** J165
[23] Zhou W J, Jin K J, Guo H Z, Ge C, He M and Lu H B 2013 *J. Appl. Phys.* **4** 1
[24] Spitzer W G, Miller R C, Kleinman D A and Howarth L E 1962 *Phys Rev* **126** 1710
[25] Guo E J, Lu H B, He M, Xing J, Jin K J and Yang G Z 2010 *Appl. Opt.* **49** 2557
[26] Zhang M, Zhang H F, Lv K B, Chen W Y, Zhou J R, Shen L and Ruan S P 2012 *Opt. Express* **20** 5936
[27] Ferrari A C, Meyer J C, Scardaci V, Casiraghi C, Lazzeri M, Mauri F, Piscanec S, Jiang D, Novoselov K S, Roth S and Geim A K 2006 *Phys. Rev. Lett.* **97** 187401
[28] Jing F Y, Zhang D Z, Li F, Zhou J R, Sun D M and Ruan S P 2015 *J. Alloys Compd.* **650** 97
[29] Gong X, Tong M H, Xia Y J, Cai W Z, Moon J S, Cao Y, Yu G, Shie C L, Nilsson B and Heeger A J 2009 *Science* **325** 1665
[30] Sablon K A, Sergeev A, Najmaei S and Dubey M 2017 *Nanophotonics* **6** 1263
[31] Nikitskiy I, Goossens S, Kufer D, Lasanta T, Navickaite G, Koppens F H L and Konstantatos G 2016 *Nat. Commun.* **7** 11954
[32] Sun Z H, Liu Z K, Li J H, Tai G A, Lau S P and Yan F 2012 *Adv. Mater.* **24** 5878
[33] Ni Z Y, Ma L L, Du S C, Xu Y, Yuan M, Fang H H, Wang Z, Xu M S, Li D S, Yang J Y, Hu W D, Pi X D and Yang D R 2017 *ACS Nano.* **11** 9854
[34] Bessonov A A, Allen M, Liu Y, Malik S, Bottomley J, Rushton A, Medina-Salazar I, Voutilainen M, Kallioinen S, Colli A, Bower C, Andrew P and Ryhänen T 2017 *ACS Nano* **11** 5547
[35] Tian H J, Liu Q L, Hu A Q, He X Y, Hu Z H and Guo X 2018 *Opt. Express* **26** 5408
[36] An X H, Liu F Z, Jung Y J and Kar S 2013 *Nano Letters* **13** 909
[37] Wang W H, Du R X, Guo X T, Jiang J, Zhao W W, Ni Z H, Wang X R, You Y M and Ni Z H 2017 *Light Sci. Appl.* **6** e17113
[38] Xu K, Xu C, Xie Y Y, Deng J, Zhu Y X, Guo W L, Xun M, Teo K B K, Chen H D and Sun J 2015 *IEEE Trans. Electron Devices* **62** 2802